Supplementary Information

Intentional Construction of High-Performance SnO_2 Catalysts with 3D Porous Structure for Electrochemical Reduction of CO_2

Xinxin Zhang,[a, b] Zhipeng Chen,[a, b] Kaiwen Mou,[a, b] Mingyang Jiao,[a] Xiangping Zhang,[c, d] and Licheng Liu*[a,d]

a CAS Key Laboratory of Bio-based Materials
Qingdao Institute of Bioenergy and Bioprocess Technology
Chinese Academy of Sciences, Qingdao 266101, Shandong, China.
E-mail: liulc@qibebt.ac.cn

b University of Chinese Academy of Sciences
Beijing 100049, China.

c Institute of Process Engineering, Chinese Academy of Sciences,
Beijing 100190, China.

d Dalian National Laboratory for Clean Energy
Dalian 116023, China.

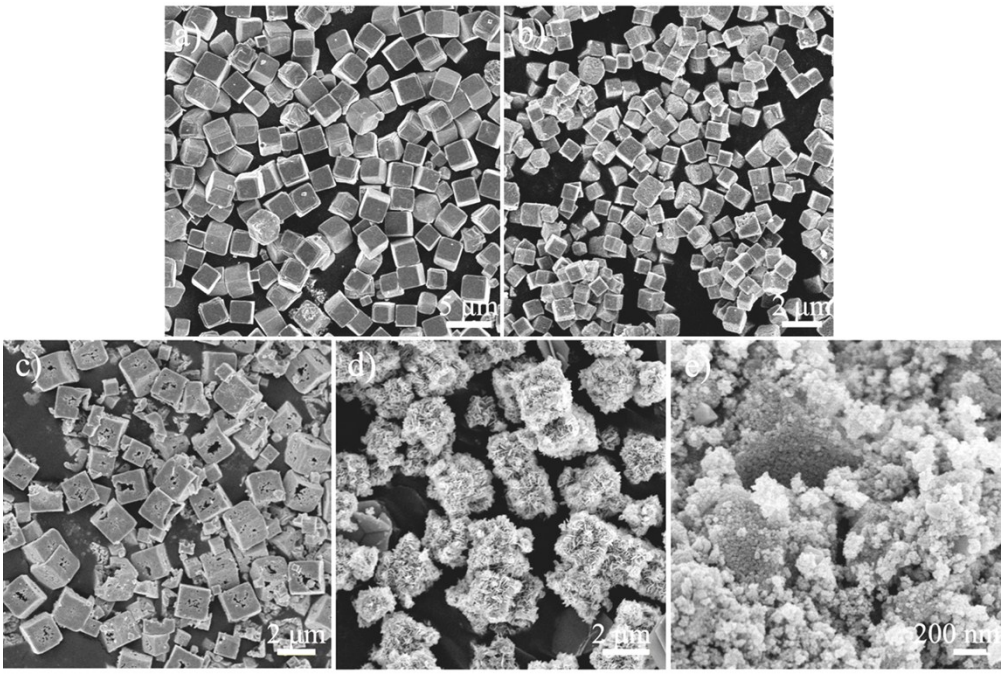

Figure S1. SEM images of $ZnSn(OH)_6$ (a), Zn_2SnO_4/SnO_2 (b), SnO_2-*NCs* (c), SnO_2-*NFs* (d) and SnO_2-*NPs* (e).

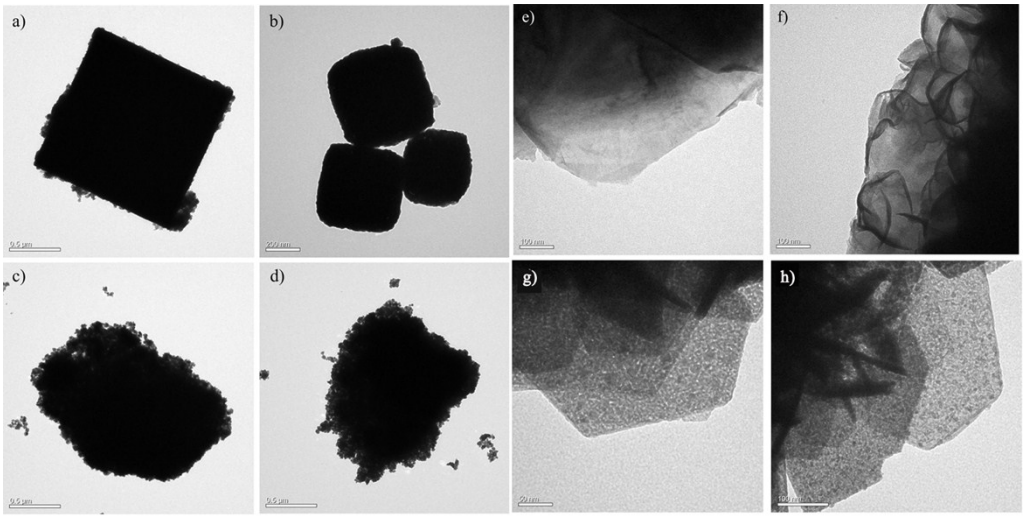

Figure S2. TEM images of $ZnSn(OH)_6$ (a), Zn_2SnO_4/SnO_2 (b), SnO_2-*NCs* (c, d), SnS_2 (e, f), SnO_2-*NFs* (g, h).

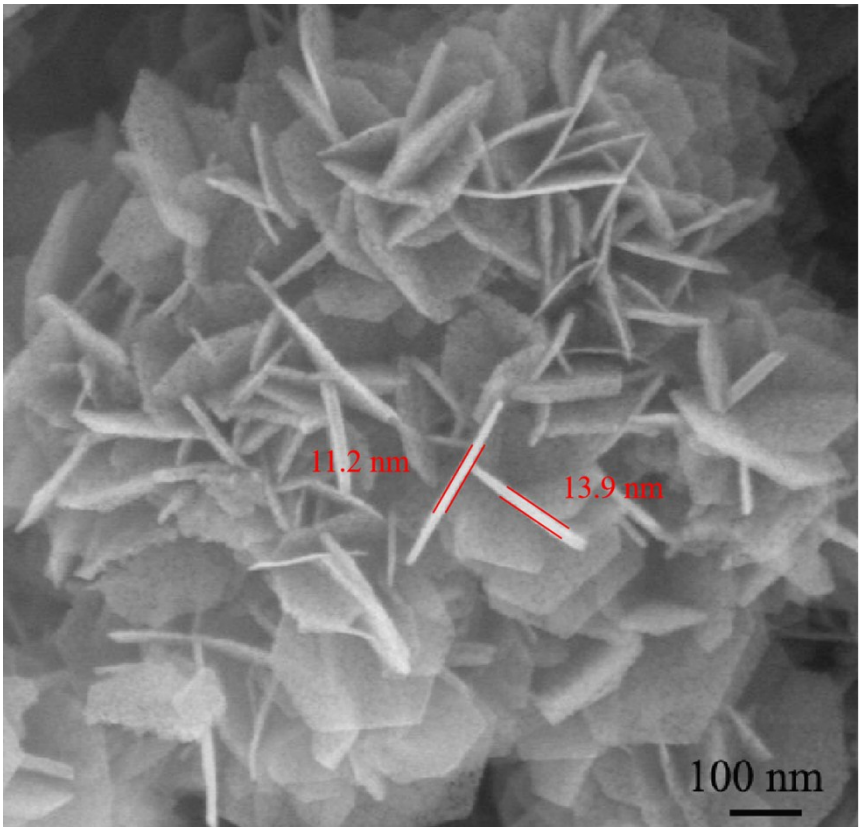

Figure S3. SEM image of SnO_2-*NFs*.

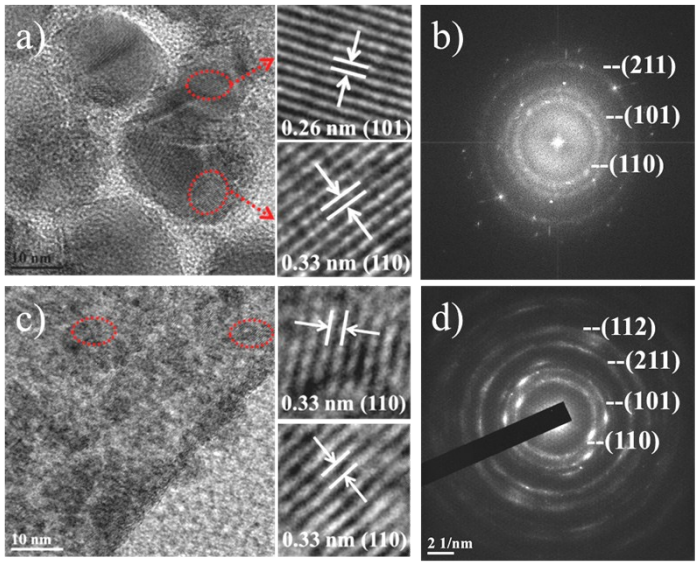

Figure S4. HRTEM images and the corresponding SAED patterns of SnO_2-*NCs* (a, b) and SnO_2-*NFs* (c, d).

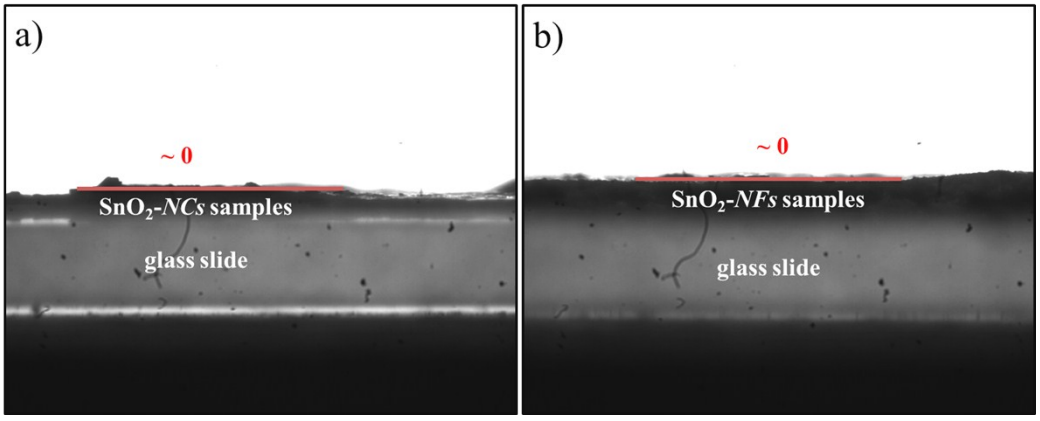

Figure S5. Contact angle of SnO_2-*NCs* and SnO_2-*NFs* samples.

The contact angles of SnO_2-*NCs* and SnO_2-*NFs* samples with 0.5M $KHCO_3$ electrolyte (3μL) were illustrated in Figure S5, indicating that the samples have the excellent wettability. Before the test, ~100mg of the SnO_2 sample powder was extruded by tablet press machine to ensure that the test surface was smooth and flat.

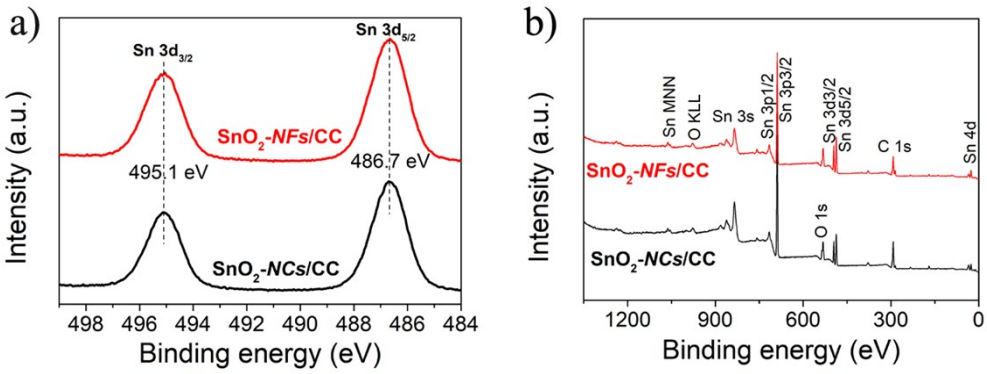

Figure S6. The Sn 3d (a) and survey (b) XPS spectra of SnO_2-*NCs* and SnO_2-*NFs* after long-term electrolysis experiments.

Figure S6 gives the typical Sn 3d XPS spectra of SnO_2-*NCs* and SnO_2-*NFs* after long-term electrolysis experiments. All samples reveal two major fitting peaks with binding energies at 495.1 eV and 486.7 eV, which could be assigned to Sn $3d_{3/2}$ and $3d_{5/2}$, respectively, and clearly confirms the Sn(IV) oxidation state of SnO_2.[1-5]

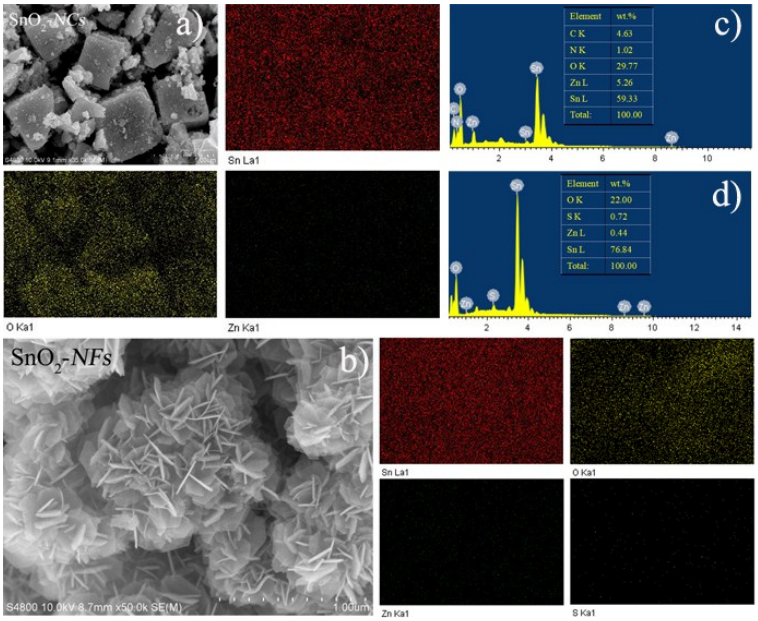

Figure S7. SEM-EDX elemental mapping images of SnO_2-*NCs* (a) and SnO_2-*NFs* (b); and the corresponding weight contents of the elements in SnO_2-*NCs* (c) and SnO_2-*NFs* (d).

SEM-EDX elemental mapping images of SnO_2-*NCs* and SnO_2-*NFs* are shown in

Figure S7. The actual distribution of Sn, Zn, O, and S elements clearly identifies. To obtain more convincing results, ICP experiment has been carried out with emphasize on Zn concentration. According to ICP results, Zn concentration is 0.22 wt. % for SnO_2-*NCs* and 0.46 wt. % for SnO_2-*NFs*, respectively.

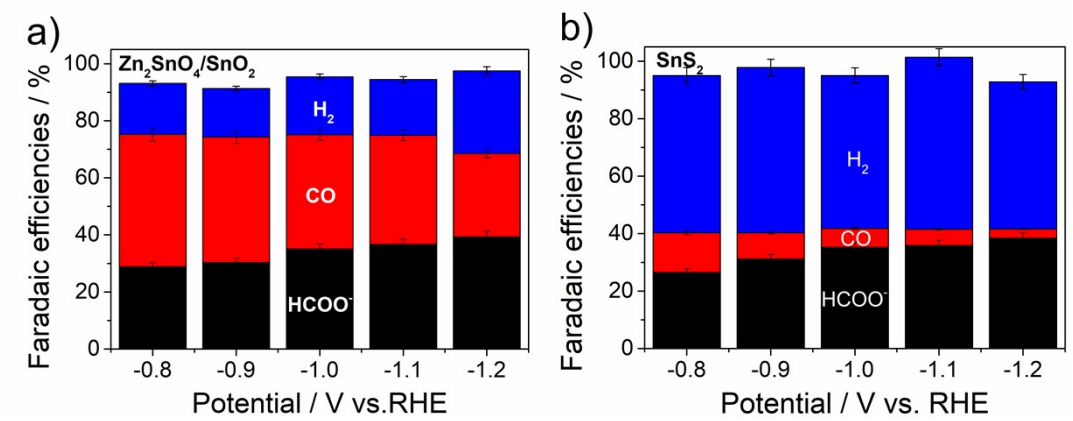

Figure S8. Faradaic efficiencies of Zn_2SnO_4/SnO_2 (a) and SnS_2 (b) catalysts at different electrolytic potentials.

Figure S8b is Faradaic efficiencies of $HCOO^-$, CO and H_2 at different electrolytic potentials on SnS_2 (the precursor of SnO_2-*NFs*, before desulfurization) sample, which shows poor performance on CO_2RR compared to SnO_2-*NFs* samples. Therefore, the activity of the electrocatlaysts is most likely from SnO_2.

Table S1. Comparison of electrocatalytic activity for electrochemical reduction of CO_2 to formate on Sn-based electrodes in an aqueous electrolyte.

Catalysts	**Overpotential (V *vs.* RHE)**	**FE (%)**	**Current density (mA cm^{-2})**	**Ref.**
Sn/SnO$_x$ Thin Film	-0.7	~97.0 C1[a] ~41.0 $HCOO^-$	-	2012 *J. Am. Chem. Soc.*[6]

nano-SnO_2/graphene	-1.8 V *vs.* SCE	>93.0	10.2 (j_{total})	2014 *J. Am. Chem. Soc.*[7]
Sn-pNWs With grain boundaries	-0.8	~80.0	4.8 (j_{HCOO^-})	2017 *Angew. Chem.*[1]
Mesoporous SnO_2-NSs/CC	~-0.97	87±2 $HCOO^-$	50 (j_{total}) 45 (j_{HCOO^-})	2017 *Angew. Chem.*[8]
SnS_2 derived Sn on rGO	-0.68	84.5	11.8 (j_{HCOO^-})	*2017 Nano Energy*[9]
Sn/CNT-Agls	-0.96	82.7	32.9 (j_{total}) 26.7 (j_{HCOO^-})	2017 *J. Mater. Chem. A*[10]
SnOx@MWCNT-COOH	-1.25 V *vs.* SHE	~100 C1 77.0 ($HCOO^-$)	9.6 (j_{total})	2019 *ChemSusChem*[11]
Sn-OH-5.9 branches	-1.6 V *vs.* Ag/AgCl	93.1 C1 82 ($HCOO^-$)	~17 (j_{total}) 10.7 (j_{HCOO^-})	2019 *J. Am. Chem. Soc.*[12]
ultra-small SnO_2-NPs (< 5 nm)	-1.21	80.0 C1 64.0($HCOO^-$)	145 (j_{total})	2018 *J. Mater. Chem. A* [13]
Sn-CNT40/ESGDEs	-1.7 V *vs.* Ag/AgCl	69.84 ± 2.41	34.21 ± 1.14	2018 *J. CO_2 Util.* [14]
PdSn/C	-0.43	99	-	2017 *Angew. Chem.*[15]
1D SnO_2 WIT	-0.89 ~ -1.29	93.0 C1 70.0 ($HCOO^-$)	-	2018 *Adv. Funct. Mater.*[16]
SnO/C (2.6 nm)	-0.86	~97.0 C1 ~70.0 ($HCOO^-$)	~28.5 (j_{total}) ~20.0 (j_{HCOO^-})	2018 *Angew. Chem.*[4]
mesoporous SnO_2	-1.15	75.0	10.8 (j_{total}) 8.2(j_{HCOO^-})	2018 *ACS Sustainable Chem. Eng.*[17]
TNS-2.0-SnO_2	-1.6	73.0	11	2018 *Adv. Energy Mater.*[18]

mesoporous-SnO_2	-0.9	83.0	16(j_{HCOO^-})	2019 *J. Mater. Chem. A* [19]
urchin-like SnO_2	-1.0 V *vs.* SHE	62.0	-	2017 *Electrochim. Acta* [20]
heat-treated Sn dendrite	-1.36	71.6	-	2015 *ChemSusChem*[21]
Sn quantum sheets confined in graphene	-1.8 V *vs.* SCE	89.0	21.1 (j_{total})	2016 *Nat. Commun.*[22]
CuOy/SnOx-CNT-#12	-1.09	79.0	6.2 (j_{HCOO^-})	2017 *ACS Appl. Mater. Interfaces* [23]
Sub-5nm SnO_2/C	-0.9	76 C1 54 ($HCOO^-$)	5.1 (j_{total}) 3.7 (j_{HCOO^-})	2018 *J. Mater. Chem. A* [24]
5 atm% Ni-doped SnS_2 nanosheets	-0.9	93 C1 80 ($HCOO^-$)	19.6	2018 *Angew. Chem.*[25]
bimetallic Bi-Sn catalyst	-1.14	96 ($HCOO^-$)	-	2018 *Adv. Energy Mater.*[26]
SnO_2/0.14@N–rGO	-0.8	89 C1	21.3 (j_{total})	*2018 Appl. Catal. B: Environ.*[5]
Au-Sn bimetallic nanoparticles	-0.9	51($HCOO^-$)	-	2019 *ACS Energy Lett.* [27]
SnO_2-*NCs*	-1.0	82.4 C1 72.6 ($HCOO^-$)	12.1(j_{total}) 9.4 (j_{HCOO^-})	This work
SnO_2-*NFs*	-1.0	91.5 C1 82.1 ($HCOO^-$)	12.9(j_{total}) 10.3 (j_{HCOO^-})	This work

[a]: C1 represents the production of $HCOO^-$ and CO.

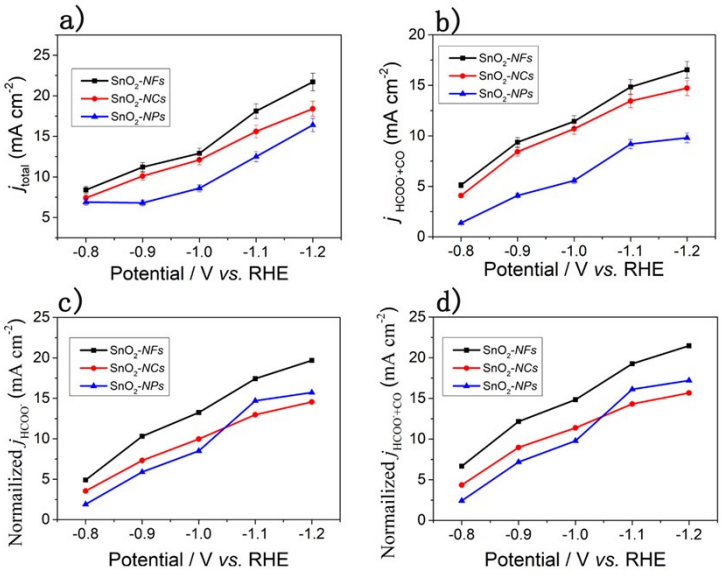

Figure S9. Total current density (a), partial (j_{HCOO^-+CO}) current density (b) and ECSA-normalized current densities (c, d) of SnO_2-*NCs*, SnO_2-*NFs* and SnO_2-*NPs*.

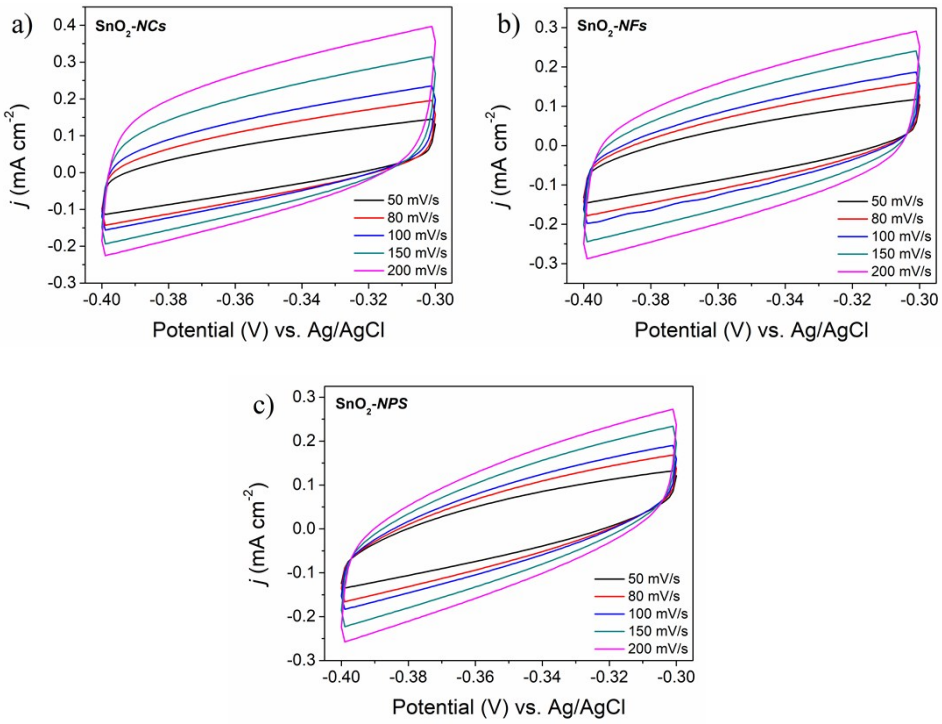

Figure S10. CV scans under different scan rates for SnO_2-*NCs* (a), SnO_2-*NFs* (b), and SnO_2-*NPs* (c).

The ECSAs of SnO_2-*NCs*, SnO_2-*NFs* and SnO_2-*NPs* electrocatalysts were evaluated by the electrochemical double-layer capacitance (Cdl), which was obtained from the

CVs (Figure S10) at different scan rates. CV measurement were performed from -0.3 to -0.4 V (*vs.* Ag/AgCl) to ensure that the location of redox peak is avoided.

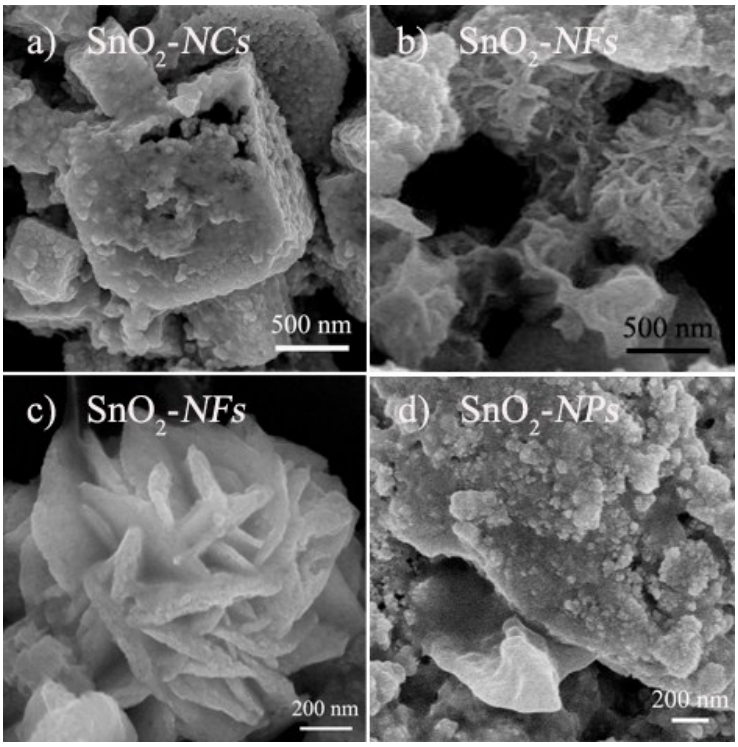

Figure S11. SEM images of the SnO_2-*NCs*/CC (a) and SnO_2-*NFs*/CC (b, c) electrode after long-term stability measurements; and freshly prepared SnO_2-*NPs*/CC (d) electrode before electrochemical test.

As shown in Figure S11, the freshly prepared SnO_2-*NPs*/CC electrode showed severe agglomeration before electrochemical test. In sharp contrast, the structure of SnO_2-*NCs*/CC and SnO_2-*NFs*/CC can be preserved to some extent after long-term stability measurements, indicating the efficient buffering effect of the 3D structure in electrolysis.

Table S2. Faradaic efficiencies of $HCOO^-$, CO, H_2 production and the total current density for the catalyst of SnO_2-NC_S, SnO_2-*NFs* and SnO_2-*NPs* at low electrolytic potentials (-0.7 V *vs.* RHE).

catalyst	FE_{HCOO^-}	FE_{CO}	FE_{H2}	j_{total}
SnO_2-*NCs*	24.1	9.4	62.0	3.9

SnO_2-*NFs*	40.5	42.9	20.2	3.6
SnO_2-*NPs*	23.8	30.9	42.0	3.2

References

1. B. Kumar, V. Atla , J. P. Brian , S. Kumari, T. Q. Nguyen, M. Sunkara and J. M. Spurgeon, *Angew. Chem. Int. Ed.*, 2017, **129**, 1-6.
2. Y. Zeng, J. Luo, Y. Wang, L. Qiao, B. Zou and W. Zheng, *Nanoscale*, 2017, **9**, 17576-17584.
3. S. Liu, J. Xiao, X. F. Lu, J. Wang, X. Wang and X. W. D. Lou, *Angew. Chem. Int. Ed.*, 2019, **58**, 8499-8503.
4. J. Gu, F. Heroguel, J. Luterbacher and X. Hu, *Angew. Chem. Int. Ed.*, 2018, **57**, 2943-2947.
5. B. Zhang, Z. Guo, Z. Zuo, W. Pan and J. Zhang, *Appl. Catal., B*, 2018, **239**, 441-449.
6. Y. Chen and M. W. Kanan, *J. Am. Chem. Soc.*, 2012, **134**, 1986-1989.
7. S. Zhang, P. Kang and T. J. Meyer, *J. Am. Chem. Soc.*, 2014, **136**, 1734-1737.
8. F. Li, L. Chen, G. P. Knowles, D. R. MacFarlane and J. Zhang, *Angew. Chem. Int. Ed.*, 2017, **56**, 505-509.
9. F. Li, L. Chen, M. Xue, T. Williams, Y. Zhang, D. R. MacFarlane and J. Zhang, *Nano Energy*, 2017, **31**, 270-277.
10. Z. Chen, S. Yao and L. Liu, *J. Mater. Chem. A*, 2017, **5**, 24651-24656.
11. J. Qiao, Q. Zhang, Y. Zhang, J. Mao, J. Liu, Y. Zhou and D. Guay, *ChemSusChem*, 2019.
12. W. Deng, L. Zhang, L. Li, S. Chen, C. Hu, Z. J. Zhao, T. Wang and J. Gong, *J. Am. Chem. Soc.*, 2019, **141**, 2911-2915.
13. C. Liang, B. Kim, S. Yang, Y. L. Yang Liu, C. Francisco Woellner, Z. Li, R. Vajtai, W. Yang, J. Wu, P. J. A. Kenis and Pulickel M. Ajayan, *J. Mater. Chem. A*, 2018, **6**, 10313-10319.
14. Q. Wang, X. Wang, C. Wu, Y. Cheng, Q. Sun and H. Yu, *J. CO_2 Util.*, 2018, **26**, 425-433.
15. X. Bai, W. Chen, C. Zhao, S. Li, Y. Song, R. Ge, W. Wei and Y. Sun, *Angew. Chem. Int. Ed.*, 2017, **56**, 12219-12223.
16. L. Fan, Z. Xia, M. Xu, Y. Lu and Z. Li, *Adv. Funct. Mater.*, 2018, **28**, 1706289.
17. R. Daiyan, X. Lu, W. H. Saputera, Y. H. Ng and R. Amal, *ACS Sustainable Chem. Eng.*, 2018, **6**, 1670-1679.
18. P. Han, Z. Wang, M. Kuang, Y. Wang, J. Liu, L. Hu, L. Qian and G. Zheng, *Adv. Energy Mater.*, 2018, **8**, 1801230.
19. N. Han, Y. Wang, J. Deng, J. Zhou, Y. Wu, H. Yang, P. Ding and Y. Li, *J. Mater. Chem. A*, 2019, **7**, 1267-1272.
20. Y. Liu, M. Fan, X. Zhang, Q. Zhang, D. Guay and J. Qiao, *Electrochim. Acta*, 2017, **248**, 123-132.
21. H. Won da, C. H. Choi, J. Chung, M. W. Chung, E. H. Kim and S. I. Woo, *ChemSusChem*, 2015, **8**, 3092-3098.

22. F. Lei, W. Liu, Y. Sun, J. Xu, K. Liu, L. Liang, T. Yao, B. Pan, S. Wei and Y. Xie, *Nat. Commun.*, 2016, **7**, 12697.
23. S. Huo, Z. Weng, Z. Wu, Y. Zhong, Y. Wu, J. Fang and H. Wang, *ACS Appl. Mater. Interfaces*, 2017, **9**, 28519-28526.
24. Y. Yiliguma, Z. Wang, C. Yang, A. Guan, L. Shang, A. M. Al-Enizi, L. Zhang and G. Zheng, *J. Mater. Chem. A*, 2018, **6**, 20121-20127.
25. A. Zhang, R. He, H. Li, Y. Chen, T. Kong, K. Li, H. Ju, J. Zhu, W. Zhu and J. Zeng, *Angew. Chem. Int. Ed.* , 2018, **57**, 10954 –10958.
26. G. Wen, D. U. Lee, B. Ren, F. M. Hassan, G. Jiang, Z. P. Cano, J. Gostick, E. Croiset, Z. Bai, L. Yang and Z. Chen, *Adv. Energy Mater.*, 2018, **8**, 1802427.
27. A. M. Ismail, G. F. Samu, Á. Balog, E. Csapó and C. Janáky, *ACS Energy Letters*, 2018, **4**, 48-53.